Reversible Accumulation of PEGylated Single-Walled Carbon Nanotubes in the Mammalian Nucleus

Jinping Cheng,[†] K. A. Shiral Fernando,[‡] L. Monica Veca,[‡] Ya-Ping Sun,[‡] Angus I. Lamond,[§] Yun Wah Lam,[†,*] and Shuk Han Cheng[†,*]

[†]Department of Biology and Chemistry, City University of Hong Kong, Hong Kong, [‡]Department of Chemistry and Laboratory for Emerging Materials and Technology, Clemson University, Clemson, South Carolina 29634-0973, and [§]Wellcome Trust Centre for Gene Regulation and Expression, College of Life Sciences, University of Dundee, Dundee DD1 5EH, Scotland, U.K.

ABSTRACT Carbon nanotubes (CNTs) have been shown to cross cell membranes and can mediate the internalization of macromolecules. These characteristics have constituted CNTs as an exciting new tool for drug delivery and biological sensing. While CNTs exhibit great potential in biomedical and pharmaceutical applications, neither the cell penetration mechanism of CNTs nor the intracellular fate of the internalized CNTs are fully understood. In this study, time-lapse fluorescence microscopy was used to investigate the intracellular distribution of FITC labeled PEGylated single-walled CNTs (FITC-PEG-SWCNTs) in living cells and shown that PEGylated SWCNTs entered the nucleus of several mammalian cell lines in an energy-dependent process. The presence of FITC-PEG-SWCNTs in the cell nucleus did not cause discernible changes in the nuclear organization and had no effect on the growth kinetics and cell cycle distribution for up to 5 days. Remarkably, upon removal of the FITC-PEG-SWCNTs from the culture medium, the internalized FITC-PEG-SWCNTs rapidly moved out of the nucleus and were released from the cells. Thus, the intracellular PEGylated SWCNTs were highly dynamic and the cell penetration of PEGylated SWCNTs appeared as bidirectional. These observations suggest SWCNTs may be used as an ideal nanovector in biomedical and pharmaceutical applications.

KEYWORDS: carbon nanotubes · nucleus · live-cell imaging · fluorescence recovery after photobleaching · cell penetration · cellular efflux

The distinctive optical, magnetic and conducting properties of nanoparticles, made from a variety of materials, have made these nanoscale substances attractive candidates in the development of new tools for molecular imaging, biosensing, and other areas of biomedical research. Carbon nanotubes (CNTs) are among the most promising nanoparticles for such applications because CNTs, unlike other types of nanomaterials, have better biocompatibility[1,2] and do not require the conjugation of antibodies or cell penetrating peptides for cell internalization.[3−5] In addition, CNTs can easily be functionalized and linked to fluorescent beacons, nucleic acids, or other small molecules.[6] These properties make CNTs an ideal candidate for a "smart" nanoparticle-based system for drug delivery and *in vivo* bioimaging. The use of CNTs in the targeted delivery of biomolecules into biological systems carries enormous medical and commercial potentials and a detailed understanding of the cell penetration mechanism and intracellular dynamics of CNTs is paramount for the development of these nanomaterials as drug delivery vehicles.[7]

Although several previous reports have demonstrated that CNTs are able to translocate across cell membrane,[4,8] the cell penetration mechanism and the intracellular dynamic fate of the internalized CNTs are not well understood. There are several possible mechanisms that have been proposed for cell penetration of CNTs. Some studies suggested that CNTs cause localized damage on the cell membrane through which cargos enter the cells.[9] Spearing has been shown to enhance this "hole-punching" process and improve the efficiency of delivery into mammalian cells.[10] On the other hand, Kam *et al.* proposed that cells take up the CNTs through an energy-requiring mechanism, such as endocytosis.[11] There is presently no consensus regarding the mechanism for the entry.

After cell penetration, the intracellular fate of the internalized CNTs appears to vary. Nuclear accumulation was observed although most related studies have reported that water soluble CNTs modified with functional groups resided in the cytoplasm upon incubation.[4,8,12,13] One study has reported that intense G-band signal was observed in the nuclear region in exposed HeLa cells using the confocal Raman imaging analysis; however, the nuclear accumulation of CNTs was not inferred because of the lack of conclusive evidence of CNT-like structures in the nucleus through ultrasections analysis under transmission electron

Ⓦ This paper contains enhanced objects available on the Internet at http://pubs.acs.org/journals/ancac3.

*Address correspondence to yunwlam@cityu.edu.hk, bhcheng@cityu.edu.hk

Received for review July 22, 2008 and accepted September 15, 2008.

Published online September 30, 2008.
10.1021/nn800461u CCC: $40.75

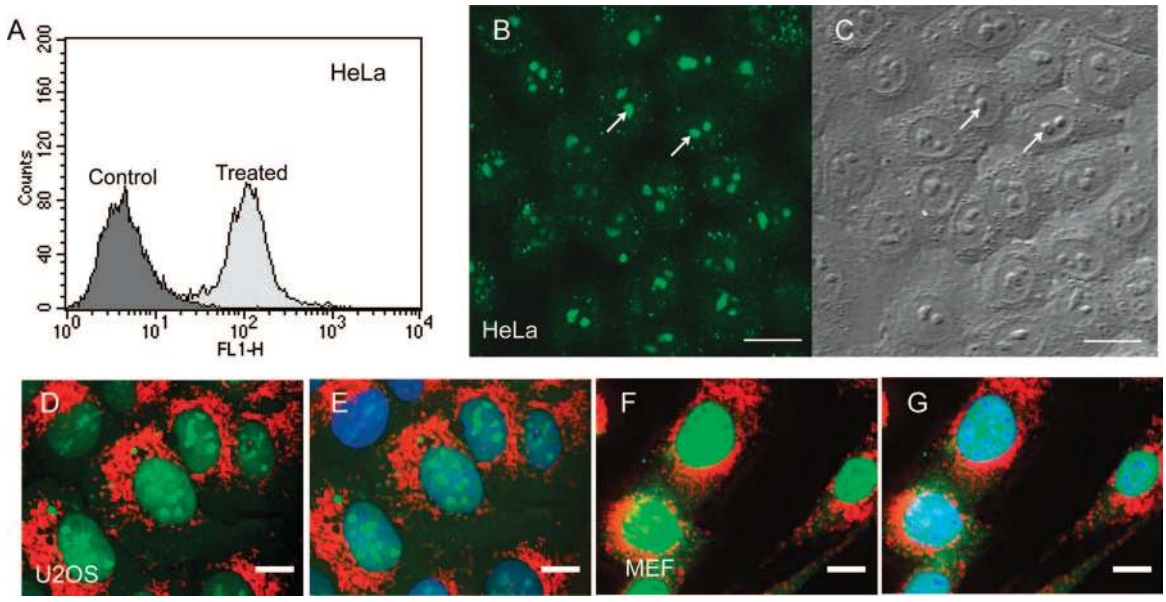

Figure 1. The cell penetration of FITC-PEG-SWCNTs and its nuclear accumulation in mammalian cells. (A) FACS analysis of HeLa cells treated with FITC-PEG-SWCNTs for 48 h showed that the treated cells took up the FITC-PEG-SWCNTs uniformly. (B) Live cell imaging showed that FITC-PEG-SWCNTs accumulated in the nucleus, mainly in the nucleolus (arrows), of HeLa cells. (C) DIC image of panel B. (D−G) U2OS cells (D, E) and MEF (F, G) were incubated with FITC-PEG-SWCNTs and then organellar markers. Signals from PEGylated SWCNTs (green) did not coincide with mitochondria (red, D−G)) but with nuclei (blue, E, G). Note that the distributions of FITC-PEG-SWCNTs between the nucleolus and the nucleoplasm are different in these three cell lines. Scale bars: (B, C) 20 μm; (D−G) 10 μm.

microscopy.[14] The nuclear accumulation of CNTs has been demonstrated by Bianco and co-workers;[8] furthermore, they reported that peptide functionalized multiwalled CNTs could cross the nuclear membrane and be successfully used for plasmid DNA delivery.[3] Previous reports focused mainly on the uptake of the CNTs and little work has been done with respect to the behaviours of CNTs after their penetration into cells. For example, intracellular transferrin-conjugated nanogold particles are known to be released from cells through exocytosis,[15] but it is not clear whether a similar process also occurs for CNTs. A better understanding of the intracellular properties of CNTs is therefore essential for the development of this nanomaterial as a drug delivery vector. In this study, nuclear accumulation of single walled CNTs conjugated with polyethylene glycol (PEG) and labeled with fluorescent dye FITC (FITC-PEG-SWCNTs) were demonstrated in several mammalian cell lines. The intracellular organization and cell division properties of the CNT-treated cells were then studied. The cellular uptake and release of FITC-PEG-SWCNTs were observed using time-lapse fluorescence microscopy. The cellular uptake of FITC-PEG-SWCNTs was compared with Texas-Red labeled Dextran as the endocytosis marker. Fluorescence after photobleaching (FRAP) was used to measure the intranuclear mobility of FITC-PEG-SWCNTs after the uptake. This work extends the current understanding of the interactions between CNTs and biological systems, such as the dynamic fate, intracellular behavior, and the uptake and release mechanism.

RESULTS AND DISCUSSION

Cell Penetration and Nuclear Accumulation of FITC-PEG-SWCNTs. FITC-PEG-SWCNTs were prepared by conjugating FITC to highly purified SWCNTs *via* PEG_{1500N} linkers (detailed information on the preparation and characterization of FITC-PEG-SWCNTs can be found in Supporting Information, supplementary Figures 1−3). We investigated the cell penetrating property of PEG-SWCNTs by incubating human cervical carcinoma cells HeLa with FITC-PEG-SWCNTs for 48 h. After extensive washing, the treated cells were analyzed by flow cytometry. As shown in Figure 1A, FITC fluorescence was detected in virtually all treated cells, suggesting that a substantial amount of FITC-PEG-SWCNTs had become associated with HeLa cells. Free FITC did not associate with HeLa cells (data not shown). The cellular association of FITC-PEG-SWCNTs was time and dose dependent (supplementary Figure 4), with cellular green fluorescence detectable as soon as after 1 h of incubation.

The detection of cellular FITC by flow cytometry suggested that PEGylated SWCNTs could either enter the cells or adhere to the cell surface. The intracellular distribution of FITC-PEG-SWCNTs in a number of mammalian cell lines was revealed by live cell fluorescence microscopy. Figure 1 panels B and C show HeLa cells incubated with FITC-PEG-SWCNTs. The green fluorescence signal was predominately in the cell nucleus with a weaker cytoplasmic staining in some cells. In most cells, FITC-PEG-SWCNTs were observed to be enriched in a few intranuclear structures. Bright-field DIC images indicated that these intranuclear structures were nucleoli (Figure 1B,C, arrows). To further characterize the sub-

cellular distribution of FITC-PEG-SWCNTs, CNT-treated cells were counterstained by a mixture of cell permeable dyes Hoechst 33342 and MitoTracker to label the nucleus and mitochrondria, respectively. The dyes were used at concentrations that did not cause detectable cell toxicity and did not interfere with normal mitosis for at least 24 h.[16,17] FITC-PEG-SWCNT was observed to coincide with Hoechst 33342 (Figure 1E,G), indicating the internalized SWCNT was predominately nuclear. This confirms that the green fluorescence detected by flow cytometry represented intracellular SWCNTs and supports previous observations that modified SWCNTs can effectively cross cell membranes.

The detection of FITC-PEG-SWCNTs in cell nucleus was observed in six mammalian cell lines (Figure 1 and supplementary Figure 5), of different histological origins, transformation status and p53 expression levels (supplementary Table 1). All of the tested cells have normal mitochondrial morphology and function, as indicated by MitoTracker staining (red in Figure 1D−G and supplementary Figure 5). The nuclear accumulation of FITC-conjugated CNTs was also observed for MWCNTs while using PEG_{1500N} as the functionalization group (data not shown), suggesting that the nuclear accumulation of PEGylated CNT is a general property of this nanomaterial. While the nuclear targeting mechanism of CNTs is not known, it is possible that the internalized PEGylated SWCNTs are retained in the nucleus through binding with specific nuclear proteins or nucleic acids. Future investigations will include the study of the effect of the molecular weight and surface coverage of PEG on the cellular uptake, intracellular distribution, and dynamic fate of CNT.

The nucleolar accumulation of FITC-PEG-SWCNTs appeared to change through time (see later) and was variable in different mammalian cell lines (Figure 1). The green fluorescence from the conjugated PEG-SWCNTs was predominately detectable in the nucleolus of HeLa cells (Figure 1B), U2OS cells (Figure 1D), and HT1080 cells (supplementary Figure 5A). However, the nucleolar accumulation of FITC-PEG-SWCNTs was not apparent in MEF (Figure 1F), C33A and HEK293 cells (supplementary Figure 5C,D).

To the best of the researchers' knowledge, PEGylated CNTs are one of the few nanomaterials that accumulate in mammalian cell nuclei without the need of cell-penetrating and nuclear-localizing tags. Several types of nanoparticles can also enter cells without any conjugation, but these nanomaterials are trapped in the endosome.[18,19] Many studies reported a predominately cytoplasmic localization of CNTs [8,12,13] instead of a nuclear accumulation. The intracellular location of different kinds of CNTs has not been systematically studied and the cause of this discrepancy is not clear.

The Cell Penetration Mechanism. To characterize the cell penetration process, FITC-PEG-SWCNTs-treated cells were exposed to a mixture of three dyes: cell permeable dyes DRAQ5[20] and MitoTracker, as well as an impermeable dye DAPI. FITC-PEG-SWCNTs-treated cells (from an incubation of 24 h) were effectively stained by both DRAQ5 and Mitotracker, but could still exclude DAPI (Figure 2A), suggesting that the internalization of FITC-PEG-SWCNTs is not a result of nonspecific membrane damages that lead to a general influx of external molecules. This result indicated that whatever the mechanism used by FITC-PEG-SWCNTs to enter cells, the plasma membrane was still intact enough to exclude a dye of 350 Daltons.

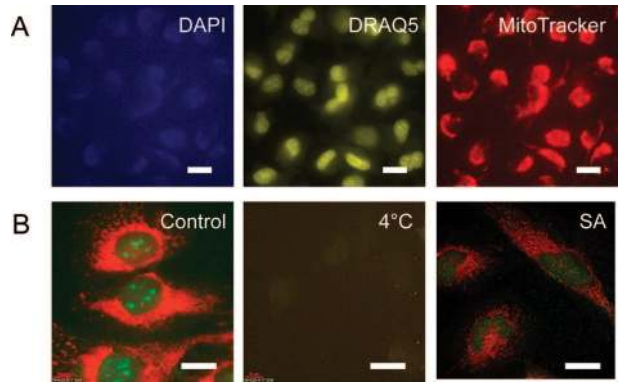

Figure 2. (A) HeLa cells excluded impermeable dye DAPI while they internalized cell permeable dyes (DRAQ5 and MitoTracker). Cells with intracellular FITC-PEG-SWCNTs (incubated for 24 h) had normal nuclear and mitochondrial morphology (DRAQ5 and MitoTracker, respectively). (B) While HeLa cells can uptake FITC-PEG-SWCNTs after coincubation for 2−3 h at 37 °C (control), they cannot take up FITC-PEG-SWCNTs efficiently at 4 °C and during energy depletion (4 °C and SA); SA = sodium azide. Scale bars: (A) 10 μm; (B) 20 μm.

To further investigate the possible mechanism for the cell penetration of PEGylated SWCNT, we studied the effect of energy depletion on its cellular uptake. Cellular internalization of FITC-PEG-SWCNTs was abolished at 4 °C and in sodium azide-treated cells (Figure 2B), indicating that the cellular uptake of PEGylated SWCNTs is an active transporting process requiring energy supply. Previous studies have suggested that mammalian cells could take up CNTs through endocytosis.[13] Here, the cellular uptake of PEGylated SWCNTs was compared with the endocytosis marker Dextran. As shown in Figure 3, after 3 h of coincubation, FITC-PEG-SWCNTs (green) located in the nucleus (Figure 3A) (verified by DRAQ5 staining, Figure 3D) while Texas-Red labeled Dextran (red) stayed in the endosomes in the cytoplasm (Figure 3B) in HeLa cells. The distinct intracellular locations of FITC-PEG-SWCNTs and Dextran indicated either SWCNTs were retained in the endosomes for much shorter time than Dextran, or that CNTs and Dextran entered the cells by different mechanisms. This experiment also suggested that the cellular uptake of CNTs did not affect the endosome function as the cells with PEG-SWCNTS could internalize Texas-Red labeled Dextran as efficiently as cells that had not been treated with CNTs (Figure 4B,C, and supplementary Figure 6).

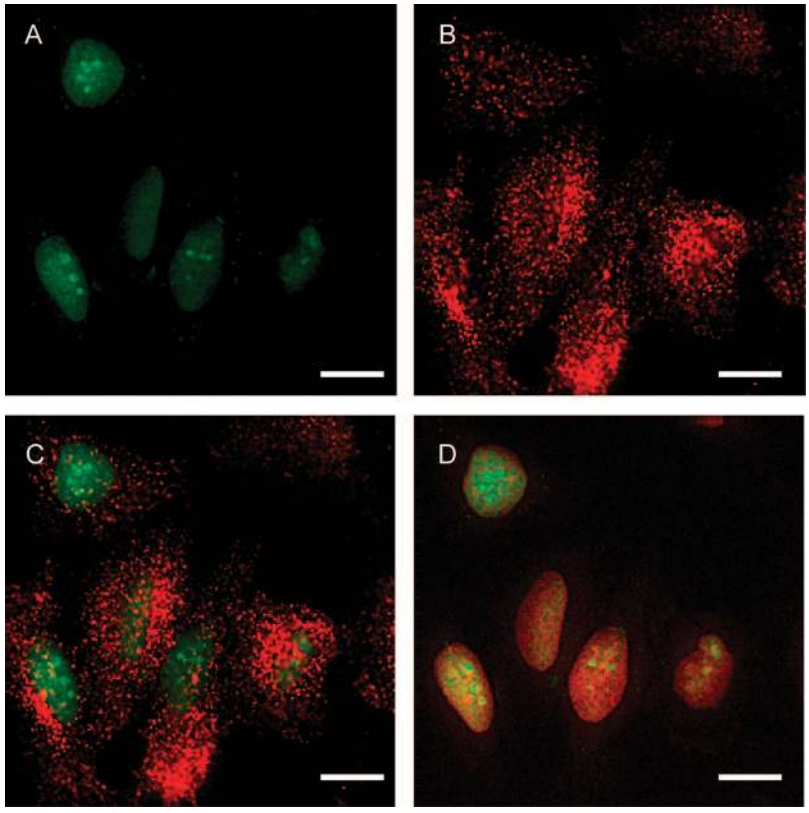

Figure 3. After incubation for 3 h, FITC-PEG-SWCNTs accumulated in the nucleus in HeLa cells (A, C, and D), but Texas-Red labeled Dextran resided in the endosomes of cytoplasm in HeLa cells (B). The green fluorescence signal from intracellular resided FITC-PEG-SWCNTs did not overlap with the red fluorescent signal from intracellular Dextran (C). But the green fluorescence signal from intracellular FITC-PEG-SWCNTs overlapped well with the signal from DNA staining using DRAQ5 (pseudocolored as red in this panel), and the overlapped part generated a yellow color in the nucleus (D). Scale bars: 10 μm.

Effect on Nuclear Organization and Cell Division. The effect of FITC-PEG-SWCNT treatment on cell proliferation was studied. Cell cycle study showed that the cellular uptake of FITC-PEG-SWCNTs did not alter the distribution of cell cycle stages after HeLa cells were exposed to PEG-SWCNTs for 48 h (Figure 4A,B). Flow cytometry analysis also did not show an obvious increase of apoptotic or multinucleated cells (Figure 4A,B and other data not shown). HeLa cells treated with PEGylated SWCNT were monitored by bright-field microscopy for 5 days (Figure 4C), and the statistical data showed that the cell number increased normally as compared to the untreated control (Figure 4D).

Time-lapse imaging showed FITC-PEG-SWCNT-treated cells went through mitosis with no observable abnormality. Figure 5 presents a time-lapse sequence that shows mitosis of mouse embryonic fibroblasts containing FITC-PEG-SWCNTs. Before mitosis, SWCNTs were enriched in the nucleus. Upon nuclear envelope breakdown at the onset of mitosis, SWCNTs became diffused throughout the entire cell during mitosis (Figure 5, arrows). At the end of the anaphase, the FITC signal accumulated in the nuclei of the daughter cells again. We did not observe any enrichment of SWCNTs on mitotic chromosomes. This suggests that SWCNTs do not exclusively bind to chromatin, but may be tethered to proteins or RNAs that are reimported into the nucleus after mitosis. It will be important in the future to identify the cellular macromolecules that interact with CNTs. To the best of the researchers' knowledge, this is the first direct visual evidence that proves CNT-treated cells can go through mitosis, hence further demonstrating that the intracellular presence of SWCNTs does not lead to activation of any major mitotic checkpoints.

Indirect immunofluorescence using antibodies specific for proteins located in nucleoli, Cajal bodies, nuclear pore complexes, splicing speckles and microtubules indicated that none of these structures were observably affected by FITC-PEG-SWCNT accumulation (Figure 6). The perinucleolar location of coilin and rounding up of splicing speckles occurred as a result of transcription inhibition.[21,22] It is inferred that transcription in the CNT-treated cells remains active because these characteristic changes in nuclear organization associated with transcription inhibition was not observed. Taken together, we did not detect any change in the intracellular structure and any discernible toxicity to cultured cells, at least within the time scale (up to 5 days) used in this study. It has been reported that exposure to SWCNTs could inhibit mitosis in human lymphocyte cultures.[23] Our data here showed, at least in cultured mammalian cells, that the presence of PEGylated SWCNTs did not appear to affect the distribution of cell cycle stages, the proliferation rate, and the nuclear structure of cells.

The Release of SWCNTs from the Cells after Internalization. The intracellular dynamics of the internalized PEGylated SWCNTs was examined by live-cell time-lapse microscopy. After incubated with FITC-PEG-SWCNTs for 24 h, HeLa cells were rinsed with fresh medium and observed with the live-cell fluorescence microscopy. The green fluorescence was predominately detectable in the nucleolus, as judged by DIC morphology (Figure 7). Time-lapse microscopy of the FITC-PEG-SWCNT-treated cells showed that the FITC fluorescence was released from the nucleolus and became diffusely distributed in the nucleus within approximately an hour after the removal of SWCNT from the medium (Figure 7). The rapid loss of nucleolar accumulation suggests that the intranuclear distribution of SWCNTs is highly dynamic and responsive to the extracellular SWCNT concentration. This phenomenon also explains the apparent difference in nucleolar SWCNT signals in HeLa cells observed in different experiments (*e.g.*, compare Figure

1B with Figure 8; the latter was imaged more than 1 h after the FITC-PEG-SWCNT treated cells were washed).

The dynamic behavior of the internalized SWCNTs after wash-out was further investigated by time-lapse microscopy. HeLa cells, treated with FITC-PEG-SWCNTs for 24 h, were washed with PBS and then stained with Mitotracker and Hoechst 33342 for 20 min in fresh cell culture medium. Figure 8A and video 1, video 2, and video 3, show that the intracellular level of FITC fluorescence (green) decreased after the removal of the FITC-PEG-SWCNTs from the medium, but the signals from DNA dye Hoechst 33342 (blue) appeared stable. The decrease of the FITC signals was not likely a result of photobleaching, because the nucleolar fluorescence, which was the strongest signal in most cells, disappeared before the fluorescence in the nucleoplasm (Figure 7 and data not shown). Importantly, during the 7 h time course, there was an increase of extracellular FITC fluorescence (Figure 8A and video 1), suggesting an extracellular accumulation of FITC-PEG-SWCNTs. By measuring the FITC signals in the same intracellular and extracellular volume through time, the decrease of the intracellular level of FITC fluorescence was shown to correspond closely with the increase in the extracellular FITC level, whereas the extracellular intensities of Hoechst 33342 and Mitotracker signals remained unchanged (Figure 8B). It is therefore inferred that the decrease of intracellular FITC-PEG-SWCNTs fluorescence was caused by the release of SWCNTs from the cells. This unexpected result implies that the translocation of SWCNTs through the plasma membrane and nuclear envelope can be bidirectional. SWCNTs are not likely to form stable, irreversible complexes with endogenous cellular structures, but can move in and out of the cell in accordance to the external SWCNT concentration. This remarkable property renders SWCNTs as an ideal vehicle for drug delivery because SWCNTs can penetrate cell membranes without causing any toxic effects, at least during the short-term (Figure 4). SWCNTs can also be removed from cells simply through washing (Figure 8), thus eliminating or reducing the potential dangers of long-term health issues caused by the cellular accumulation of SWCNTs.

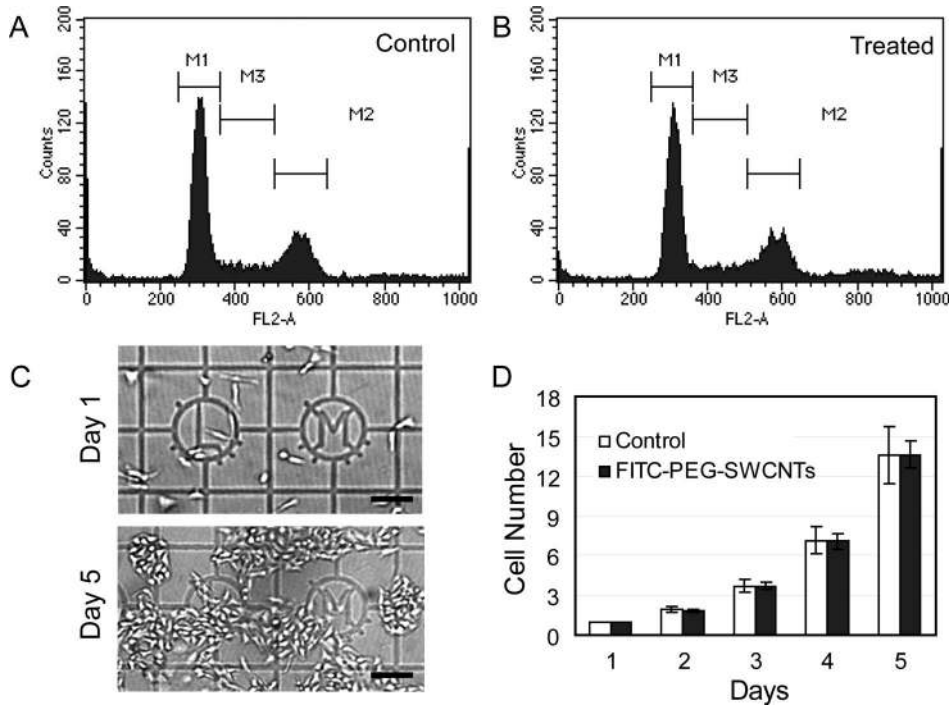

Figure 4. Flow cytometry cell cycle analysis of the propidium iodide-stained untreated HeLa cells (A) and cells incubated with FITC-PEG-SWCNTs for 48 h (B) showed that the treated cells had similar cell cycle distribution compared to the control. The proliferation analysis showed that proliferation rates of HeLa cells that were exposed to FITC-PEG-SWCNTs for up to 5 days are similar to the untreated cells (D). The cell number was measured by counting the number of cells per square (shown in panel C) every 24 h. The graph of panel C showed an example of the proliferation assay that was imaged, in the same region of the coverslip that HeLa cells were cultured for 1 day (day 1) and 5 days (day 5) after treatment with FITC-PEG-SWCNTs. Note the absence of dead cells.

FRAP Analysis for Intracellular SWCNTs. To confirm that this intracellular distribution of FITC fluorescence

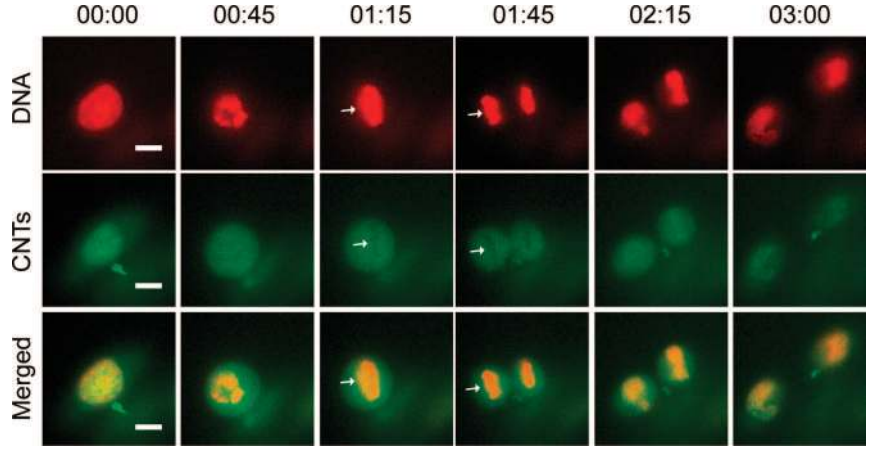

Figure 5. The intracellular localization of FITC-PEG-SWCNTs did not affect cell division. Time-lapse sequence showing the mitosis of mouse embryonic fibroblasts treated with FITC-PEG-SWCNTs for 24 h (middle panels). The mitotic chromosomes were labeled with DRAQ5 (pseudocolored as red, upper panels). Note that CNTs were excluded from mitotic chromosomes (white arrows). Scale bars correspond to 10 μm.

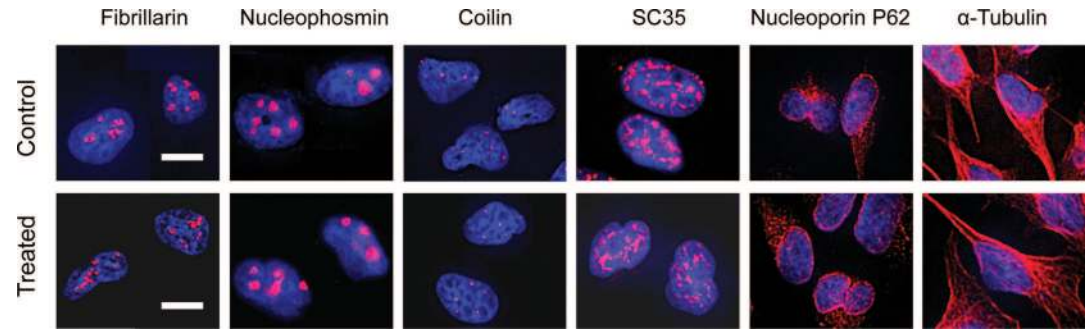

Figure 6. Internalization of FITC-PEG-SWCNTs for 48 h caused no detectable changes in the morphology of the nucleolus (Fibrillarin, nucleophosmin), Cajal bodies (Coilin), splicing speckles (SC35), the nuclear envelope (Nuclearporin p62), and microtubules (α-Tubulin). Scale bars correspond to 10 μm.

faithfully reported the localization of SWCNTs and was not due to free FITC generated by the breakdown of the internalized SWCNTs, FRAP analysis was performed on the FITC-PEG-SWCNT-treated cells. HeLa cells were treated with FITC-PEG-SWCNTs for 48 h and washed, and the FITC fluorescence in a small nuclear region was then photobleached (Figure 9A, upper panels). The subsequent recovery in fluorescence in the photobleached region measures the intranuclear mobility of the fluorescent molecules, which in turn depends on the size of the macromolecular complex that contain this fluorescent label.[24] Figure 9B (red curve) shows the FRAP measurement of nuclear FITC-PEG-SWCNT signals. The recovery half-time was more than 1 min, which is comparable to many typical protein complexes in the human nucleus,[25] and is considerably slower than free, unbound molecules, such as GFP.[26,27] Next, we delivered FITC-PEG-SWCNTs directly into HeLa cells by bead loading, a technique commonly used for introducing macromolecules into cells through reversible damages to plasma membrane caused by glass beads.[28] Like the PEGylated SWCNTs that entered cells physiologically, the bead-loaded SWCNTs also localized in the cell nucleus, with enrichment in the nucleolus (Figure 9A, middle panels), whereas bead-loaded FITC distributed evenly throughout the cells (Figure 9A, lower panels). This suggests that FITC-PEG-SWCNTs can be targeted to the nucleus regardless of the cell penetration methods.

FRAP analyses were performed on cells immediately after being bead-loaded with FITC-PEG-SWCNTs. As shown in Figure 9B (green curve), the kinetics of fluorescence recovery of the bead-loaded FITC-PEG-SWCNTs was virtually indistinguishable from that of FITC-PEG-SWCNTs physiologically internalized by cells. This indicates that an exposure of FITC-PEG-SWCNTs to the intracellular environment for 48 h did not affect their mobility. In contrast, FRAP measurement of free FITC introduced into HeLa cells by bead loading[28] (Figure 9A, lower panels, and Figure 9B, blue curve) showed a much poorer bleaching efficiency and a much faster recovery than FITC-PEG-SWCNT. This is consistent with the extremely fast mobility of the small FITC molecules, a phenomenon well-documented for other small, freely diffusing fluorophores such as unconjugated GFP.[29−31] Taken together, observations by FRAP analysis showed further evidence that the intracellular FITC signals were from the intact PEG-SWCNTs and intracellular SWCNTs were dynamic.

CONCLUSIONS AND PERSPECTIVES

The potential widespread use of CNTs has led to a strong public concern about the impact of these new nanomaterials on human health and the environment. Information concerning the potential biological effects that are related to CNTs is still insufficient. Our study suggested that well-purified SWCNTs, functionalized with PEG_{1500N}, resided in the intracellular nucleus and were nontoxic to cultured mammalian cells upon exposure. Previous cytotoxicity study of CNTs gave rise to much controversy. Contaminants associated with CNTs have been shown to induce in-

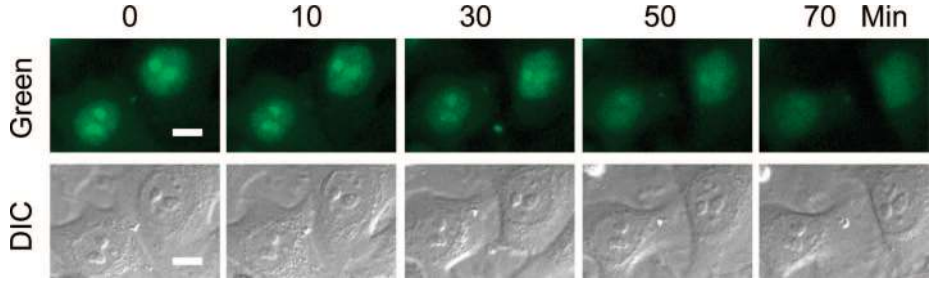

Figure 7. Intracellular distribution and dynamics of FITC-PEG-SWCNTs in HeLa cells. Time-lapse sequence showing the change of the intracellular distribution of FITC-PEG-SWCNTs (incubated for 24 h) in HeLa cells after the removal of the SWCNTs in the culture medium. The numbers on top indicate the time after the removal of SWCNTs from the medium (in minutes). Scale bars: 10 μm.

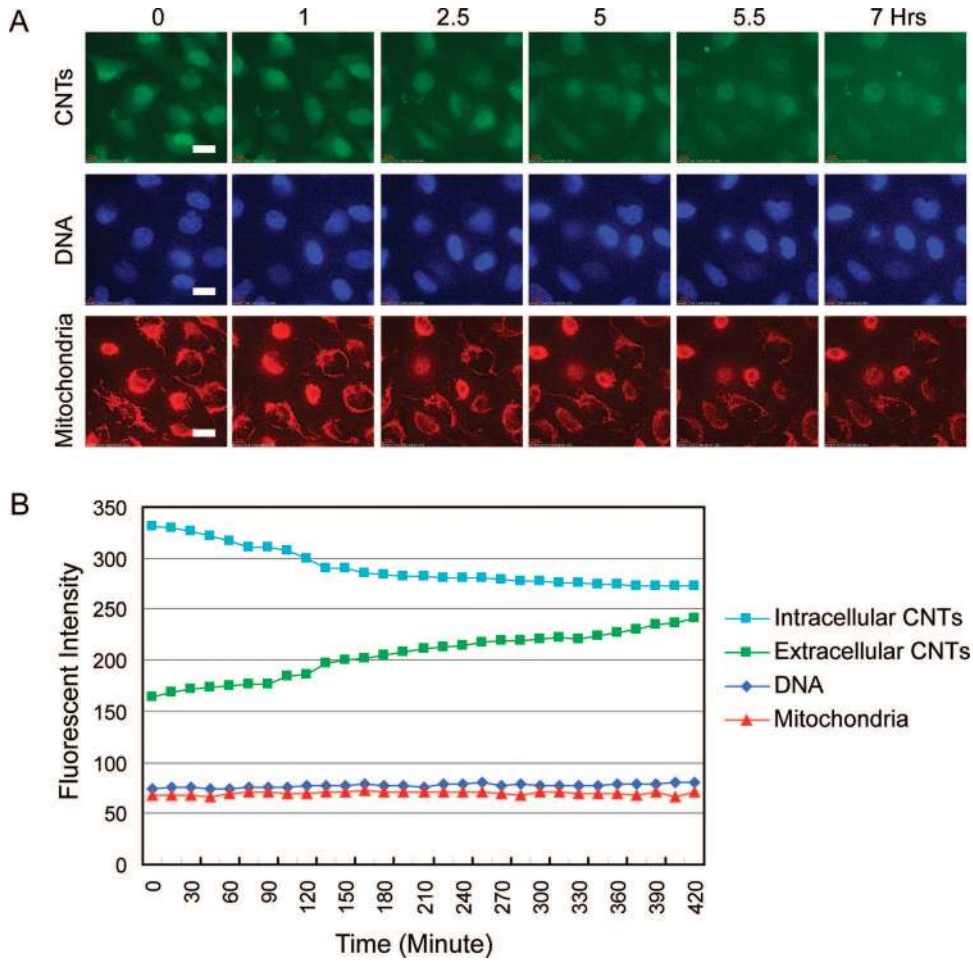

Figure 8. Release of the intracellular FITC-PEG-SWCNTs after the cell internalization. (A) HeLa cells were incubated with FITC-PEG-SWCNTs (green) for 24 h and stained with Hoechst 33342 (blue) and MitoTracker (red) before time-lapse imaging for 7 h in fresh medium. (B) Quantitative analysis of the fluorescence signals in panel A. One region in the extracellular space was selected and the intensities of signals from FITC-PEG-SWCNTs (green data points), MitoTracker (red data points), and Hoechst 33342 (blue data points) were measured. An area of the same size was selected in the intranuclear space and the intensity of the FITC-PEG-SWCNTs (cyan data points) was measured. Scale bars correspond to 20 μm.

Ⓦ Video 1 shows the direct observation of the release of FITC-PEG-SWCNTs from the SWCNT-treated cells.

Ⓦ Video 2 shows the stable distribution of DNA.

Ⓦ Video 3 shows mitochondria markers in the same SWCNT-treated cells.

tracellular oxygen species,[32] whereas highly purified CNTs are less toxic[33] or even nontoxic.[1] The conflicting information sometimes was due to the technical problems when common cytotoxicity assays were applied for CNTs.[34] For example, MTT assay was commonly used to study cell proliferation, but it will generate a fake cytotoxic effect since SWCNTs appear to interact with tetrazolium salts such as MTT.[34] Here we studied the cell proliferation by direct cell number counting using live-cell imaging with the aid of the marked coverslips. This proliferation study through imaging analysis avoided potential nonspecific chemical interactions and is more direct.

In this study, FITC was used to label the PEGylated SWCNTs in living cultured mammalian cells, and time-lapse live-cell microscopy was used to characterize the behavior of SWCNTs after cell entry. It was assumed that FITC, being a biological inactive dye, did not affect the intracellular behaviours of SWCNTs. Future studies will be done using the intrinsic optical properties of SWCNTs to study the intracelluar fate and cell uptake. Here, we have shown that FITC-PEG-SWCNTs accumulated in the nucleus, mainly in the nucleolus in some cell lines, the site of ribosomal biogenesis,[35,36] and were highly dynamic inside the cells. It has been shown that through live-cell time-lapse imaging and immunofluorescence, the architecture of the nucleus for cells treated with PEG-SWCNTs were not detectably affected. Since the organization of the cell nucleus is functionally linked to the regulation of gene expression and is known to be deformed in cells with abnormal metabolism,[37,38] it is inferred that the normal

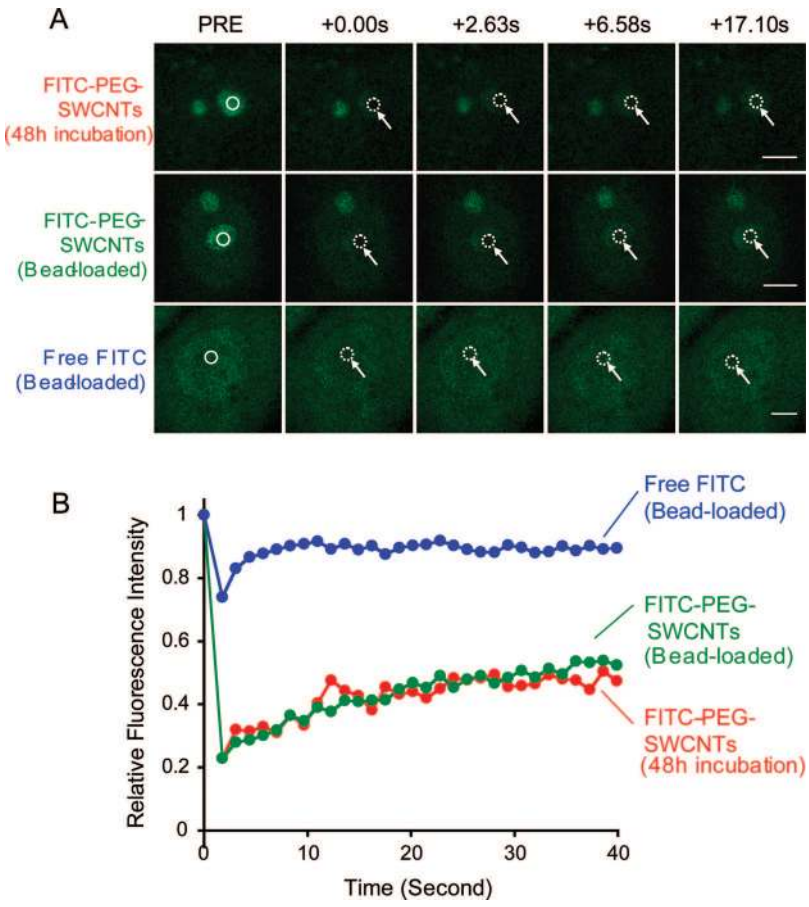

Figure 9. FRAP analysis of the intracellular FITC-PEG-SWCNTs. (A) Small regions (dotted circles) in the nuclei of live HeLa cells containing FITC-PEG-SWCNTs internalized after an incubation of 48 h (upper panels), FITC-PEG-SWCNTs internalized as a result of bead loading (middle panels) and bead-loaded free FITC (lower panels) were photobleached. The fluorescence intensities in the circled regions were monitored by time-lapse imaging over at least 40 s. Numbers on top indicate the time after photobleaching (in seconds). Scale bars: 5 μm. (B) Recovery of fluorescence intensities in the bleached areas (relative to the prebleached levels) over time: blue data points, free FITC; green data points, bead-loaded FITC-PEG-SWCNTs; red data points, FITC-PEG-SWCNTs internalized by incubation for 48 h.

nuclear structure of SWCNT-treated cells is further evidence that the intracellular accumulation of SWCNTs does not harbor any serious toxicity.

The behavior of FITC-PEG-SWCNTs, as revealed by FRAP, is similar to most nuclear proteins studied[25,39] and is consistent with the view that the mammalian nucleus has a highly crowded microenvironment in which macromolecules form transient, but specific interactions with each other.[40] The FRAP analysis that has been reported is the first study of its kind on CNT and can be used as the basis for further characterizations of the intracellular behavior in nanoparticles. SWCNTs can also be used for investigating the intranuclear environment, such as molecular crowding, using optical and other biophysical methodologies.[41]

This study has examined the intracellular and dynamic fate of internalized FITC-PEG-SWCNTs in mammalian cells. Remarkably, the intranuclear distribution of SWCNTs depended on the extracellular concentration of SWCNTs. When PEGylated SWCNTs were removed from the culture medium, the nucleolar SWCNTs rapidly moved to the rest of the nucleus and were eventually released from the cells. This concentration-dependent cellular accumulation of chemicals has been described for some nuclear dyes,[42] but has never been directly observed for nanoparticles. This remarkable property suggests a possible controllable clearance of SWCNTs after the completion of delivery. The controllable entrance and release of SWCNTs by setting intracellular and extracellular conditions provide strong support that SWCNTs may be an ideal tool to be used as nanovectors in biomedical and pharmaceutical applications.

METHODS AND EXPERIMENTS

Preparation and Characterization of PEGylated SWCNTs. SWCNTs were purchased from Carbon Solutions, Inc. The CNT purification, functionalization, and characterization for SWCNTs have been reported elsewhere.[6,43] For purification, SWCNTs were first burned in the furnace at 300 °C in air for 30 min to remove the amorphous carbon and then were further purified by refluxing in an aqueous HNO_3 solution (2.6 M, 48 h), washing repeatedly with water for 3 days, and drying. The samples after purification were validated with thermogravimetric analysis, electron microscopy, and Raman characterization. Nanotube-bound carboxylic acids were then used to attach aminopolymers polyethylene glycol (PEG) to the nanotubes *via* amide linkages.[44] The PEG-SWCNTs were luminescent and the visible/near-IR absorption spectra of the as-purified SWCNTs and PEGylated SWCNTs were also studied. The PEG-SWCNTs were then labeled with fluorescent dye fluorescein isothocyanate (FITC) to facilitate biological imaging. Detailed information on the preparation and characterization of SWCNT samples can be found in Supporting Information.

Cell Culture, Incubation of Living Cells in Nanotube Solutions and Microscopy. Human adenocarcinoma cells (HeLa, ATCC No: CCL2), human cervical cancer cell (C33A, ATCC No: HTB31), human embryonic kidney cells (HEK293, ATCC No: CRL1573), human sarcoma cells (HT1080, ATCC No: CC1121), human bone osteosarcoma cells (U2OS, ATCC No: HTB96), and mouse embryonic fibroblast (MEF, ATCC No: SCRC1008.2) were purchased from American-type Culture Collection (ATCC, VA, USA) and cultured in Dulbecco's modified Eagle's medium (Invitrogen, UK) with 10% fetal bovine serum (Invitrogen, UK). For live-cell imaging experiments, cells grown in chambered coverglasses (Lab-Tek 155411, NUNC) were mounted on a wide-field fluorescence microscope (DeltaVision Spectris; Applied Precision, UK) that was fitted with an environmental chamber (Solent Scientific) to maintain temperature at 37 °C and a Cool Snap charge-coupled device camera (Roper Scientific). Some additional images (*e.g.*, Figure 1B,C) were taken on a Leica TCS SP5 confocal microscope.

The FITC-PEG-SWCNTs were diluted in culture medium to 55 μg/mL (CNT's equivalent concentration) and incubated for durations that are indicated in the study figures. After the incubation with PEGylated SWCNTs, the cells in some experiments were stained for 20 min with Hoechst 33342 (0.25 μg/ml, Sigma) or DRAQ5 (5 μM, cell-permeant far-red fluorescence DNA probe, Biostatus) or DAPI (0.25 μg/ml, Sigma), and MitoTracker (25 nM, Molecular Probes). After the staining, the staining solution was removed and the cells were washed with cell culture medium for 5 min, three times.

Before imaging, growth medium was replaced with a custom-made phenol red-free, CO_2 independent medium (Invitrogen, UK). In all experiments, an Olympus 40× oil immersion lens (NA 1.35) was used. DIC imaging was implemented with the appropriate prism insert (Olympus). For time-lapse live-cell imaging, ten optical sections (1.2 μm each) were collected at regular intervals of 5 min with an exposure time of 35 ms. All images were recorded using a binning of 2 × 2 on the CH350 charge-coupled device camera, yielding an effective pixel size of 0.102 μm × 0.102 μm.

The microscopy images were viewed as three-dimensional sum projections (Figure 4C), single optical sections (Figures 5, 6, 7, and 8) or maximum intensity projections (Figures 1D−G, 2 and 3 and supplementary Figure 5). Data analysis was performed using the SoftWoRx image processing program (Applied Precision, UK), with additional analysis (Figure 9 and supplementary Figure 4) performed using MetaMorph (Universal Imaging).

FRAP Photokinetic Experiments. The FRAP experiments were performed on a Leica TCS SP5 confocal microscope. To briefly summarize, small regions in the cells were photobleached using a 488 nm laser (100% laser power for 0.3 s) and time-lapse sequences of single optical sections were collected by bidirectional scanning using 10% of laser power for about 40 s at the interval of about one image per second. The FRAP data were measured by the built-in Leica software LAS LF and plotted using Excel. Bead loading of FITC-PEG-SWCNTs and FITC was completed as described.[28] Cells were analyzed by FRAP within 30 min after bead loading.

ATP Depletion Experiments. The ATP depletion was conducted with 10 mM sodium azide (Sigma, s-8032). The cells were incubated with the ATP depletion drug and FITC-PEG-SWCNTs for 2−3 h simultaneously. After the coincubation, the cells were washed and incubated with the same ATP depletion CO_2 independent culture medium (Invitrogen) before the live cell staining and imaging. The mitochondria were stained as the marker of the ATP supply with MitoTracker (25 nM, Molecular Probes). The uptake of the PEG-SWCNTs was visualized with green fluorescent signal.

The incubation of HeLa cells with FITC-PEG-SWCNTs was carried out in the cold room with a temperature of 4 °C with CO_2 independent culture medium (Invitrogen). The control group of the cells was cultured in a 37 °C incubator with CO_2-independent culture medium (Invitrogen). The Texas-Red labeled Dextran (Invitrogen) was used as the positive control of the endocytosis uptake and was coincubated with the cells together with PEG-SWCNTs after 3 h of incubation; live-cell imaging was recorded as above.

Antibodies, Fixation, Immunofluorescence, and Imaging. All fixation, permeabilization, and immunostaining were performed at room temperature. Cells grown on glass coverslips were washed in phosphate buffered saline (PBS) and fixed for 10 min with freshly made 4% paraformaldehyde in PBS. Permeabilization was performed with 0.5% Triton X-100 in PBS for 10 min. Cells were subsequently washed three times in PBS and then blocked with 10% goat serum in PBS for 20 min before incubated with primary antibody for 1 h. Three washes with PBS were carried out before incubation with affinity-purified Texas red-conjugated goat antimouse secondary antibody (Jackson ImmunoResearch Laboratories) for 45 min. Finally, cells were stained with DAPI (0.3 μg/ml; Sigma). After a final set of washes, cells were mounted in Vectashield media (Vector Laboratories).

The following antibodies were used in the study. Fibrillarin was detected by mouse monoclonal antibody 72B9 (1:25, a generous gift from Professor E.M. Tan, Scripps Institute). Nucleoporin was detected by mouse monoclonal antibody 414 (1:100, Convance). Splicing factor SC35 was detected by mouse monoclonal antibody anti-SC35 (1:100, Sigma S4045). Coilin was detected by monoclonal antibody 5P10 (1:25). Nucleophosmin was detected by mouse monoclonal antibody anti-B23 (1:100, Sigma B0566); microtubules were detected by mouse anti-α-tubulin DM1A monoclonal antibody (1:100, Sigma T6199).

Immunostained specimens were examined by using a 40× NA 1.3 Plan-Apochromat objective. Three-dimensional images were recorded on a Zeiss DeltaVision Restoration microscope (Applied Precision, UK) that was equipped with a three-dimensional motorized stage and a Photometrics CH350 camera containing a 1401E charge-coupled device (Eastman Kodak Co., UK). For each sample, 10 optical sections separated by 0.2 μm were recorded. Exposures were chosen so that images yielded gray scale units between 200 and 2000, remaining well above the camera dark current, but below the 4096-U maximum.

Cell Proliferation Assay and Flow Cytometry. The cells were seeded one day earlier on a grid coverslip (Eppendorf Cellocate Square size 175 μm) in a 60 mm dish (Merck no. 402/0322/12). The cells were incubated with PEG-SWCNTs continuously for 4 days. The same areas on the coverslip, recognized by grid coordination, were imaged using a 10× lens (Zeiss Planneofluar, NA 0.30 every 24 h during the 4 day period. The cell number in the imaged area was counted. This method allows repeated measurements of the same cell populations over time and is therefore more accurate than comparing averages of different cell populations.

Cells were analyzed by using a flow cytometry (FACS, Becton Dickinson) after incubation in various nanotube solutions. The cells were fixed with cold 70% ethanol and then stained with 50 μg/ml propidium iodide (P3566, Invitrogen) supplemented with 50 μg/ml RNase A (Roche). Dual detection of red fluorescence was carried out with the fixed cells for the cell cycle analysis and green fluorescence with the live cells for the uptake analysis. The data that is presented in this study represents the mean red and green fluorescence obtained with a population of 10000 cells.

Acknowledgment. The work described in this paper was substantially supported by a grant from the Research Grants Council of the Hong Kong SAR (Project No. CityU 160108). The Clemson group was supported by the U.S. National Science Foundation. A. I. Lamond is a Wellcome Trust principal investigator. L. Qu is thanked for experimental assistance and the Cheng, Sun, and Lamond groups for fruitful discussions and comments.

Supporting Information Available: Supplementary figures and tables; detailed preparation and characterization of PEGylated SWCNTs; purification and functionalization procedures; TGA and AFM details. This material is available free of charge *via* the Internet at http://pubs.acs.org.

REFERENCES AND NOTES

1. Zanello, L. P.; Zhao, B.; Hu, H.; Haddon, R. C. Bone Cell Proliferation on Carbon Nanotubes. *Nano Lett.* **2006**, *6*, 562–567.
2. Dumortier, H.; Lacotte, S.; Pastorin, G.; Marega, R.; Wu, W.; Bonifazi, D.; Briand, J. P.; Prato, M.; Muller, S.; Bianco, A. Functionalized Carbon Nanotubes are Non-Cytotoxic and Preserve the Functionality of Primary Immune Cells. *Nano Lett.* **2006**, *6*, 1522–1528.
3. Pantarotto, D.; Singh, R.; McCarthy, D.; Erhardt, M.; Briand, J. P.; Prato, M.; Kostarelos, K.; Bianco, A. Functionalized Carbon Nanotubes for Plasmid DNA Gene Delivery. *Angew. Chem., Int. Ed.* **2004**, *43*, 5242–5246.
4. Shi Kam, N. W.; Jessop, T. C.; Wender, P. A.; Dai, H. Nanotube Molecular Transporters: Internalization of Carbon Nanotube-Protein Conjugates Into Mammalian Cells. *J. Am. Chem. Soc.* **2004**, *126*, 6850–6851.
5. Wu, W.; Wieckowski, S.; Pastorin, G.; Benincasa, M.; Klumpp, C.; Briand, J. P.; Gennaro, R.; Prato, M.; Bianco, A. Targeted Delivery of Amphotericin B to Cells by Using Functionalized Carbon Nanotubes. *Angew. Chem., Int. Ed.* **2005**, *44*, 6358–6362.

6. Sun, Y. P.; Fu, K. F.; Lin, Y.; Huang, W. J. Functionalized Carbon Nanotubes: Properties and Applications. *Acc. Chem. Res.* **2002**, *35*, 1096–1104.
7. Lin, Y.; Taylor, S.; Li, H. P.; Fernando, K. A. S.; Qu, L. W.; Wang, W.; Gu, L. R.; Zhou, B.; Sun, Y. P. Advances Toward Bioapplications of Carbon Nanotubes. *J. Mater. Chem.* **2004**, *14*, 527–541.
8. Pantarotto, D.; Briand, J. P.; Prato, M.; Bianco, A. Translocation of Bioactive Peptides Across Cell Membranes by Carbon Nanotubes. *Chem. Commun.* **2004**, 16–17.
9. Rojas-Chapana, J.; Troszczynska, J.; Firkowska, I.; Morsczeck, C.; Giersig, M. Multi-Walled Carbon Nanotubes for Plasmid Delivery into *Escherichia coli* Cells. *Lab Chip* **2005**, *5*, 536–539.
10. Cai, D.; Mataraza, J. M.; Qin, Z. H.; Huang, Z.; Huang, J.; Chiles, T. C.; Carnahan, D.; Kempa, K.; Ren, Z. Highly Efficient Molecular Delivery into Mammalian Cells Using Carbon Nanotube Spearing. *Nat Methods* **2005**, *2*, 449–454.
11. Kam, N. W.; Liu, Z.; Dai, H. Carbon Nanotubes as Intracellular Transporters for Proteins and DNA: An Investigation of the Uptake Mechanism and Pathway. *Angew. Chem., Int. Ed.* **2006**, *45*, 577–581.
12. Monteiro-Riviere, N. A.; Nemanich, R. J.; Inman, A. O.; Wang, Y. Y.; Riviere, J. E. Multi-Walled Carbon Nanotube Interactions with Human Epidermal Keratinocytes. *Toxicol. Lett.* **2005**, *155*, 377–384.
13. Kam, N. W.; Dai, H. Carbon Nanotubes as Intracellular Protein Transporters: Generality and Biological Functionality. *J. Am. Chem. Soc.* **2005**, *127*, 6021–6026.
14. Yehia, H. N.; Draper, R. K.; Mikoryak, C.; Walker, E. K.; Bajaj, P.; Musselman, I. H.; Daigrepont, M. C.; Dieckmann, G. R.; Pantano, P. Single-Walled Carbon Nanotube Interactions with HeLa Cells. *J. Nanobiotechnol.* **2007**, *5*, 1–17.
15. Chithrani, B. D.; Chan, W. C. Elucidating the Mechanism of Cellular Uptake and Removal of Protein-Coated Gold Nanoparticles of Different Sizes and Shapes. *Nano Lett.* **2007**, *7*, 1542–1550.
16. Trinkle-Mulcahy, L.; ersen, J.; Lam, Y. W.; Moorhead, G.; Mann, M.; Lamond, A. I. Repo-Man Recruits PP1 Gamma to Chromatin and is Essential for Cell Viability. *J. Cell Biol.* **2006**, *172*, 679–692.
17. Kimura, H.; Cook, P. R. Kinetics of Core Histones in Living Human Cells: Little Exchange of H3 and H4 and Some Rapid Exchange of H2B. *J. Cell Biol.* **2001**, *153*, 1341–1353.
18. Duan, H.; Nie, S. Cell-Penetrating Quantum Dots Based on Multivalent and Endosome-Disrupting Surface Coatings. *J. Am. Chem. Soc.* **2007**, *129*, 3333–3338.
19. Gemeinhart, R. A.; Luo, D.; Saltzman, W. M. Cellular Fate of a Modular DNA Delivery System Mediated by Silica Nanoparticles. *Biotechnol. Prog.* **2005**, *21*, 532–537.
20. Martin, R. M.; Leonhardt, H.; Cardoso, M. C. DNA Labeling in Living Cells. *Cytometry A* **2005**, *67*, 45–52.
21. Carmo-Fonseca, M.; Pepperkok, R.; Carvalho, M. T.; Lamond, A. I. Transcription-Dependent Colocalization of the U1, U2, U4/U6, and U5 snRNPs in Coiled Bodies. *J. Cell Biol.* **1992**, *117*, 1–14.
22. Haaf, T.; Ward, D. C. Inhibition of RNA Polymerase II Transcription Causes Chromatin Decondensation, Loss of Nucleolar Structure, and Dispersion of Chromosomal Domains. *Exp. Cell Res.* **1996**, *224*, 163–173.
23. Szendi, K.; Varga, C. Lack of Genotoxicity of Carbon Nanotubes in a Pilot Study. *Anticancer Res.* **2008**, *28*, 349–352.
24. Houtsmuller, A. B.; Vermeulen, W. Macromolecular Dynamics in Living Cell Nuclei Revealed by Fluorescence Redistribution After Photobleaching. *Histochem. Cell Biol.* **2001**, *115*, 13–21.
25. Dundr, M.; Hoffmann-Rohrer, U.; Hu, Q.; Grummt, I.; Rothblum, L. I.; Phair, R. D.; Misteli, T. A Kinetic Framework for a Mammalian RNA Polymerase *in vivo*. *Science* **2002**, *298*, 1623–1626.
26. Griffis, E. R.; Altan, N.; Lippincott-Schwartz, J.; Powers, M. A. Nup98 is a Mobile Nucleoporin with Transcription-Dependent Dynamics. *Mol. Biol. Cell* **2002**, *13*, 1282–1297.
27. Swaminathan, R.; Hoang, C. P.; Verkman, A. S. Photobleaching Recovery and Anisotropy Decay of Green Fluorescent Protein GFP-S65T in Solution and Cells: Cytoplasmic Viscosity Probed by Green Fluorescent Protein Translational and Rotational Diffusion. *Biophys. J.* **1997**, *72*, 1900–1907.
28. McNeil, P. L.; Warder, E. Glass Beads Load Macromolecules into Living Cells. *J. Cell Sci.* **1987**, *88*, 669–678.
29. Sprague, B. L.; McNally, J. G. FRAP Analysis of Binding: Proper and Fitting. *Trends Cell Biol.* **2005**, *15*, 84–91.
30. Ali, G. S.; Reddy, A. S. ATP Phosphorylation and Transcription Regulate the Mobility of Plant Splicing Factors. *J. Cell Sci.* **2006**, *119*, 3527–3538.
31. Christensen, M. O.; Barthelmes, H. U.; Feineis, S.; Knudsen, B. R.; Andersen, A. H.; Boege, F.; Mielke, C. Changes in Mobility Account for Camptothecin-Induced Subnuclear Relocation of Topoisomerase I. *J. Biol. Chem.* **2002**, *277*, 15661–15665.
32. Pulskamp, K.; Diabate, S.; Krug, H. F. Carbon Nanotubes Show no Sign of Acute Toxicity but Induce Intracellular Reactive Oxygen Species in Dependence on Contaminants. *Toxicol. Lett.* **2007**, *168*, 58–74.
33. Nimmagadda, A.; Thurston, K.; Nollert, M. U.; McFetridge, P. S. F. Chemical Modification of SWNT Alters *in vitro* Cell-SWNT Interactions. *J. Biomed. Mater. Res., Part A* **2006**, *76A*, 614–625.
34. Worle-Knirsch, J. M.; Pulskamp, K.; Krug, H. F. Oops They Did it Again! Carbon Nanotubes Hoax Scientists in Viability Assays. *Nano Lett.* **2006**, *6*, 1261–1268.
35. Boisvert, F. M.; van, K. S.; Navascues, J.; Lamond, A. I. The Multifunctional Nucleolus. *Nat. Rev. Mol. Cell Biol.* **2007**, *8*, 574–585.
36. Lam, Y. W.; Trinkle-Mulcahy, L.; Lamond, A. I. The Nucleolus. *J. Cell Sci.* **2005**, *118*, 1335–1337.
37. Jackson, D. A.; Pombo, A.; Iborra, F. The Balance Sheet for Transcription: an Analysis of Nuclear RNA Metabolism in Mammalian Cells. *FASEB J.* **2000**, *14*, 242–254.
38. Leonhardt, H.; Rahn, H. P.; Cardoso, M. C. Functional Links Between Nuclear Structure, Gene Expression, DNA Replication, and Methylation. *Crit Rev. Eukaryot. Gene Expr.* **1999**, *9*, 345–351.
39. Chen, D.; Huang, S. Nucleolar Components Involved in Ribosome Biogenesis Cycle Between the Nucleolus and Nucleoplasm in Interphase Cells. *J. Cell Biol.* **2001**, *153*, 169–176.
40. Misteli, T. The Concept of Self-Organization in Cellular Architecture. *J. Cell Biol.* **2001**, *155*, 181–185.
41. Richter, K.; Nessling, M.; Lichter, P. Experimental Evidence for the Influence of Molecular Crowding on Nuclear Architecture. *J. Cell Sci.* **2007**, *120*, 1673–1680.
42. Frias, J. C.; Bobba, G.; Cann, M. J.; Hutchison, C. J.; Parker, D. Luminescent Nonacoordinate Cationic Lanthanide Complexes as Potential Cellular Imaging and Reactive Probes. *Org. Biomol. Chem.* **2003**, *1*, 905–907.
43. Huang, W. J.; Fernando, S.; Allard, L. F.; Sun, Y. P. Solubilization of Single-Walled Carbon Nanotubes with Diamine-Terminated Oligomeric Poly(ethylene glycol) in Different Functionalization Reactions. *Nano Lett.* **2003**, *3*, 565–568.
44. Huang, W. J.; Taylor, S.; Fu, K. F.; Lin, Y.; Zhang, D. H.; Hanks, T. W.; Rao, A. M.; Sun, Y. P. Attaching Proteins to Carbon Nanotubes *via* Diimide-Activated Amidation. *Nano Lett.* **2002**, *2*, 311–314.